SENSOR DATA FUSION AND SUBMERGED TEST RESULTS OF A PECTORAL FIN PROPELLED UUV

Jason D. Geder[1]
Ravi Ramamurti[1]
John Palmisano[2]
Marius Pruessner[2]
Banahalli Ratna[2]
William C. Sandberg[3]

[1] Laboratory for Computational Physics and Fluid Dynamics, Naval Research Laboratory, Washington, DC 20375
[2] Center for Bio-molecular Science and Engineering, Naval Research Laboratory, Washington, DC 20375
[3] Modeling and Analysis Division, Technology and Advanced Systems Business Unit, Science Applications International Corporation, McLean, VA 22102

Abstract

An inertial navigation system (INS) complete with extended Kalman filters (EKFs) to mitigate sensor measurement errors is described in this paper for a six-degree-of-freedom (6-DOF) pectoral fin propelled unmanned underwater vehicle (UUV). Simulation results are discussed and the vehicle model is validated with initial experimental data.

After modeling the sensor performance characteristics, EKFs are implemented to fuse imperfect gyroscope and accelerometer data from the INS and eliminate the integration errors caused by measurement biases of these sensors. Vehicle responses to standard maneuvers are simulated including straight line motion, constant radius turn, and climbing. In addition to simulating the vehicle with sensor models in the loop, an updated set of control laws is shown to be robust with respect to variations in actuator performance.

The control architecture designed and tested in simulation, which utilizes combinations of fin kinematics sets as well as fin rotation biases to generate desired control force vectors, is implemented in the vehicle onboard microcontroller. This paper addresses initial results of our submerged test vehicle utilizing two updated control techniques. Evaluation of results reveals agreement between experimental and simulated results in vehicle speed and maneuverability which serves to validate our model.

1. Introduction

Low-speed and high-maneuverability performance, required in near-shore and littoral zone missions, is a major weakness of current unmanned underwater vehicle (UUV) technology. To address this issue, flapping fin mechanisms have been studied to understand how certain aquatic organisms achieve their high levels of controllability (Lauder and Jayne (1996), Walker and Westneat (1997)). Several investigators have adapted passively deforming flapping fins onto UUVs (Kato (1999, 2000), Hobson et al (1999)). Also, investigators have been pursuing the development of actively controlled, deformable flapping fins (Ando et al (2006), Palmisano et al (2007, 2009), Tangorra et al (2008)).

In our previous work, we concluded that actively controlled-curvature biomimetic pectoral fins were the solution for low-speed, high-maneuverability operation of UUVs (Ramamurti and Sandberg (2006)). We constructed such a fin propulsor (Palmisano et al (2007)), designed a test vehicle that utilizes two of these fins for propulsion and control

(Geder et al (2007)), and have improved vehicle performance through implementation of two novel pectoral fin control methods (Geder et al (2008), Palmisano et al (2009)).

This paper improves the fidelity of our vehicle model, and validates this model through preliminary experimental testing of the fins on our test vehicle. The vehicle 6-DOF model is refined to include an onboard inertial navigation system (INS) and fin actuator characteristics. In support of this new model, extended Kalman filters (EKFs) are implemented to fuse imperfect gyroscope and accelerometer data from the INS and eliminate the integration errors caused by measurement biases of these sensors. The model is also corrected to include the latest fin force production results over a range of fin kinematics that were presented by Ramamurti et al. (2009).

To accommodate this updated model, necessary changes are made to the feedback control laws, and simulated results again demonstrate desired vehicle performance. This new set of control laws is robust with respect to actuator performance, as variation up to 50% from predicted thrust production only leads to very small changes in vehicle response.

In addition to discussing modeling and control simulation improvements, this paper also addresses initial results of our submerged test vehicle. The control architecture, which utilizes combinations of fin kinematics sets as well as fin rotation biases to generate desired control force vectors, is implemented in the onboard microcontroller. Initial submerged vehicle test results show good agreement with simulated results. Differences between experimental and simulated results are accounted for, and the vehicle responses are used to drive the design of a four-fin hover capable vehicle.

2. Vehicle Design and Modeling

2.1. Design Overview

The test vehicle designed by Geder et al (2007) carries a set of two Naval Research Laboratory (NRL) actively controlled-curvature fins and provides a means of demonstrating force production and controllability of the fins in an underwater test environment. The hull (Figure 1) measures 1.3″ high, 13″ long and 7″ wide, and it has a dry weight of 2.2 pounds. Key hull design considerations included manufacturability, vertical plane stability, and drag reduction.

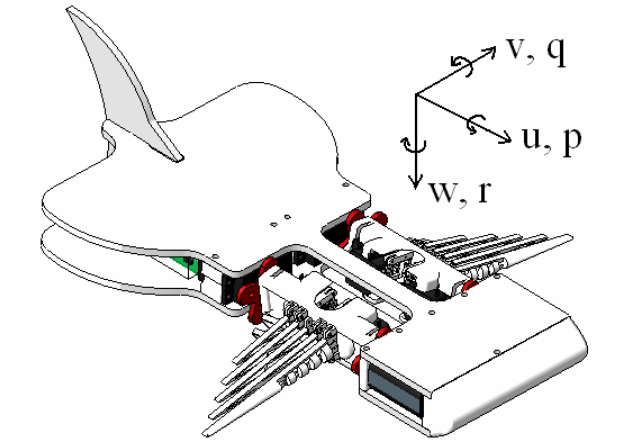

Fig. 1. Two-fin test vehicle showing fins, fixed vertical and horizontal tails, and vehicle body axes.

The horizontal flat hull design was easy to manufacture, and provides a high pitch moment of inertia improving stability in the vertical plane. To reduce vehicle drag and to better understand the flow field about the vehicle, computational fluid dynamic (CFD) analysis was used during the design process. Stabilizing surfaces including vertical and horizontal fixed tails were added to reduce yaw motion and further damp pitch oscillation.

A three-axis accelerometer, two-axis gyro, tilt compensated compass, and a depth sensor are used to provide vehicle state feedback to an ATmega2560 microcontroller. This microcontroller commands outputs to both fins based on processed sensor data, and can transmit real-time data wirelessly.

2.2. Vehicle Sensor Model

The original model of the test vehicle is outlined by Geder et al (2007) including six-degree-of-freedom (6-DOF) equations of motion and vehicle coefficient derivation aided by CFD force analysis. These initial vehicle equations lacked sensor models to account for inaccuracies in measurement of vehicle states needed in control of the vehicle.

The sensor models outlined here are based off both product data sheets and our experimental analysis of each sensor. Measured output of the ADXL330 three-axis accelerometer and the IDG300 two-axis gyro using an 8-bit analog to digital conversion (ADC) is shown in Figures 2 and 3. This data is used to map sensor measurements to vehicle states, and to compute measurement sensitivity of these devices.

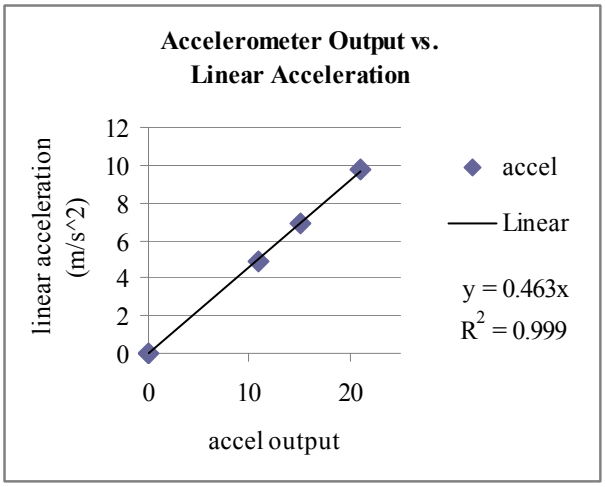

Fig. 2. Experimental data mapping accelerometer output to linear accelerations along each of the three sensor axes.

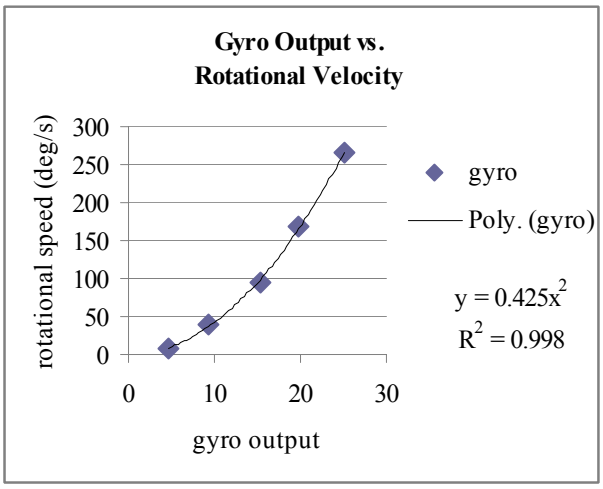

Fig. 3. Experimental data mapping gyroscope outputs to rotational velocities about each of the two sensor axes.

True linear acceleration varies linearly with the accelerometer output, and we see in Figure 2 that this device has a sensitivity of 0.46 m/s^2 with 8-bit ADC. Actual rotational velocity varies with the square of gyroscope output, and we see in Figure 3 that this device has a sensitivity of 0.85·(gyro output) °/s with 8-bit ADC.

On the two-fin vehicle, accelerometer axes are aligned with the body *uvw* axes, and the gyro axes are aligned with the *uv* axes (about which *p* and *q* are taken). These axes are shown in Figure 1.

A capacitor is added to the outputs of the ADXL330 to create a low-pass filter for noise reduction. Based on the equation for cutoff frequency,

$$f_c = \frac{1}{2\pi RC}, \tag{1}$$

and the presence of a 32 kΩ resistor built into the ADXL330 chip, a 0.1 μF capacitor is added to each output to implement a 50 Hz bandwidth filter.

The IDG300 gyro has a 140 Hz low-pass filter built in, and only requires a 2 kHz external low-pass filter to attenuate high-frequency noise from vibration.

The pressure sensor is also an analog sensor, and the data is similarly converted to a digital signal. The equation for depth as determined from the data sheet for the pressure sensor and the pressure at various water depths is,

$$Depth,(meters) = \frac{\left(PSout_{8-bit}(x) - PSout_{8-bit}(1atm)\right)}{22.5} \tag{2}$$

where $PSout_{8\text{-}bit}$ is the 8-bit pressure sensor data output. This indicates a sensitivity of 0.044 meters, or ~1.75 inches.

The compass is a digital sensor used to measure heading, and it has built in tilt compensation based on accelerometer readings. According to the data sheet, heading accuracy is +/- 1° for tilt angles under 15°. As the tilt angle increases, heading accuracy drops to a maximum of +/- 2°. Experimental testing of the compass has confirmed this output accuracy measured at near zero tilt angles, as shown in Figure 4.

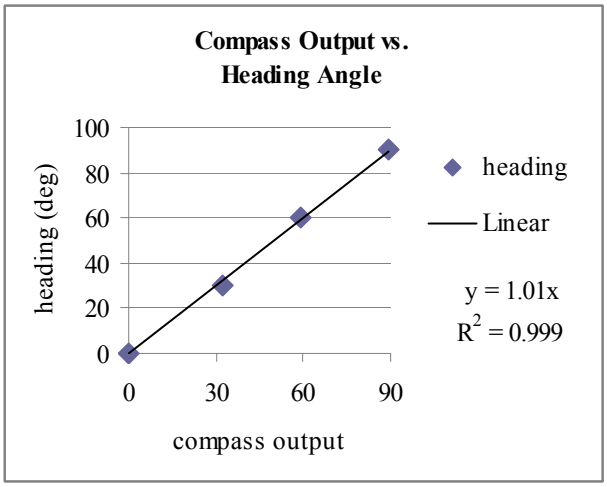

Fig. 4. Experimental data mapping compass output to heading of the vehicle.

3. Sensor Data Fusion

On our vehicle, roll and pitch angles are derived from gyro rate integration. Due to biases in the sensor calibration, these attitude (defined as vehicle pitch and roll) errors will experience unbounded growth leading to long-term instability. However, augmenting gyro integrated angles with accelerometer based angle measurements ensures attitude errors will be bounded.

For nonlinear dynamic systems, EKFs have long served as the standard choice for fusing sensor data to eliminate the effects of inherent errors in the sensor readings (Lefferts et al (1982), Uhlmann (1992)). This type of filter estimates true system states by calculating sensor correction weights based on an estimate of statistical variance.

The two angles we are interested in estimating for our EKF system, roll (φ) and pitch (θ), compose the state vector, $\boldsymbol{x}$. The input vector, $\boldsymbol{u}$, is comprised of vehicle angular rates, and the output vector, $\boldsymbol{z}$, is comprised of vehicle body frame accelerations as given in Equation 3.

$$\vec{x} = \begin{bmatrix} \varphi \\ \theta \end{bmatrix}, \qquad \vec{u} = \begin{bmatrix} p \\ q \\ r \end{bmatrix}, \qquad \vec{z} = \begin{bmatrix} a_x \\ a_y \\ a_z \end{bmatrix} \tag{3}$$

Because we only have two axes of gyro rate measurements, for the EKF system r will be calculated from the derivative of the compass measurements. For our discrete-time system, we write the state transition and observation equations as,

$$\begin{aligned} \vec{x}_k &= f(x_{k-1}, u_k) + w_k \\ \vec{z}_k &= h(x_k) + v_k \end{aligned}, \tag{4}$$

where $\boldsymbol{w}_k$ is the process noise with covariance Q_k and $\boldsymbol{v}_k$ represents the measurement noise with covariance R_k. Our formulation of the EKF is a simplification on the process implemented by Eldredge (2006) detailing the estimation of pitch and roll for a 6-DOF vehicle. More specifically, we do not include a vehicle speed term in estimating linear accelerometer measurements. We eliminate this vehicle speed term because the slow linear speeds and angular rates experienced by our vehicle make this term negligible. This estimate gives us for $f(x,u)$ and $h(x)$,

$$\begin{aligned} f(x,u) &= \begin{bmatrix} p + q\sin\varphi\tan\theta + r\cos\varphi\tan\theta \\ q\cos\varphi - r\sin\varphi \end{bmatrix} \\ h(x) &= \begin{bmatrix} g\sin\theta \\ -g\sin\varphi\cos\theta \\ -g\cos\varphi\cos\theta \end{bmatrix} \end{aligned} \tag{5}$$

Estimating the values for Q_k and R_k determines the weighting given to the sensor measurements involved in the state estimation. The process noise varies with the rotational motion of the vehicle, while the measurement noise varies with the accelerations experienced by the vehicle. We have estimated the terms in Q_k and R_k based on sensor noise density, or noise per unit of bandwidth, as,

$$\begin{aligned} Q_k &= \begin{bmatrix} \sigma_{Q,k}^2 & 0 \\ 0 & \sigma_{Q,k}^2 \end{bmatrix} = \begin{bmatrix} 0.1 & 0 \\ 0 & 0.1 \end{bmatrix} \\ R_k &= \begin{bmatrix} \sigma_{R,k}^2 & 0 & 0 \\ 0 & \sigma_{R,k}^2 & 0 \\ 0 & 0 & \sigma_{R,k}^2 \end{bmatrix} = \begin{bmatrix} 10 & 0 & 0 \\ 0 & 10 & 0 \\ 0 & 0 & 10 \end{bmatrix} \end{aligned} \tag{5}$$

An example response for estimating pitch angle, θ, is given in Figure 5. True angle is computed in simulation from 6-DOF equations. We see in this response that although the gyro integrated angle diverges from the true angle, our EKF estimate continues to track the actual angle.

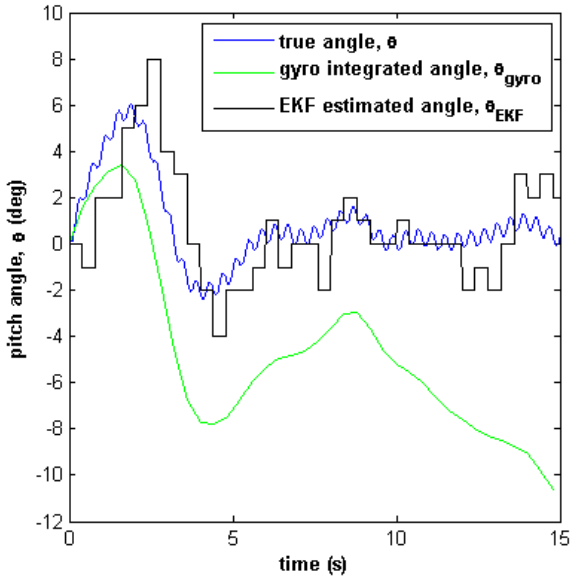

Fig. 5. Extended Kalman filter estimate of vehicle pitch angle showing good tracked while gyro integrated estimate drifts.

The 0.4 second output rate of the EKF estimated angle in Figure 5 is driven by the flapping frequency of the fins. Vehicle kinematics update once every full cycle based on the output of the onboard controller.

Beyond attitude estimation, a method of dead reckoning is used to determine position which can be updated with periodic positioning measurements to correct for errors. This has been designed, but has not been built or tested on our vehicle, so the focus of this paper is on accurately estimating vehicle attitude.

4. Vehicle Test Results

With the sensor models and attitude estimation EKF built into the vehicle model, simulations were run to test stability and various maneuvering capabilities. Some of these simulations were validated by submerged tests of the constructed vehicle.

4.1. Straight Line Maneuver

A straight line simulation was done to determine stability using the EKF to maintain zero pitch and roll angles, and to measure maximum vehicle forward speed. The results in Figure 6b indicate the vehicle was able to reach a speed of 0.35 m/s after ~5 seconds starting from hover, averaging 0.3 m/s over a 15 second simulation. Stability was maintained and true vehicle orientation was confined to variations of less than 2° from commanded values in steady state (Figure 6a).

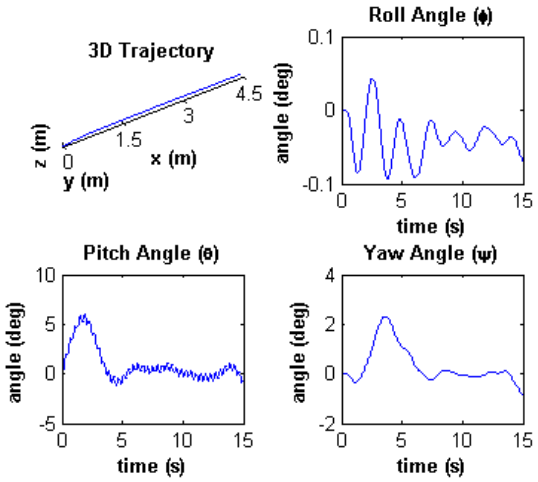

(a)

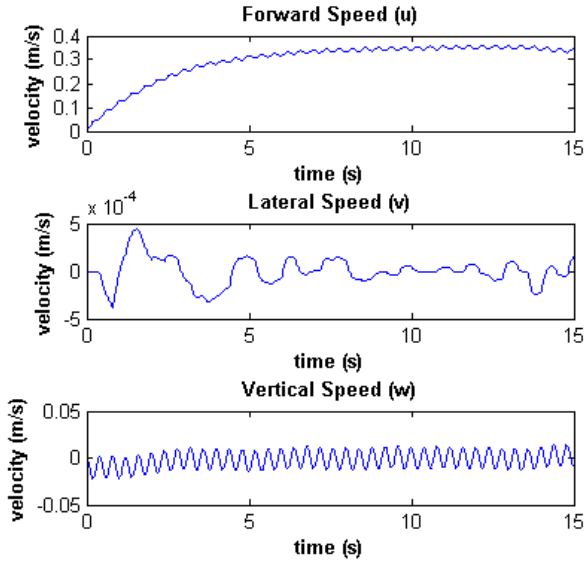

(b)

Fig. 6. Simulated forward speed test showing (a) trajectory and attitude stability, and (b) 0.35 m/s top speed of the vehicle.

The experimental results of a straight line test showed the actual vehicle moved slightly slower than predicted, averaging about 0.24 m/s over a 10 second interval starting from hover. In the simulation, the vehicle averaged 0.28 m/s through the first 10 seconds, a 14% difference. Experimental drag was greater than simulated drag due to an addition of externally mounted Styrofoam to correct for unexpected buoyancy imbalances, and unkempt external wiring due to the nature of the prototype (Figure 7).

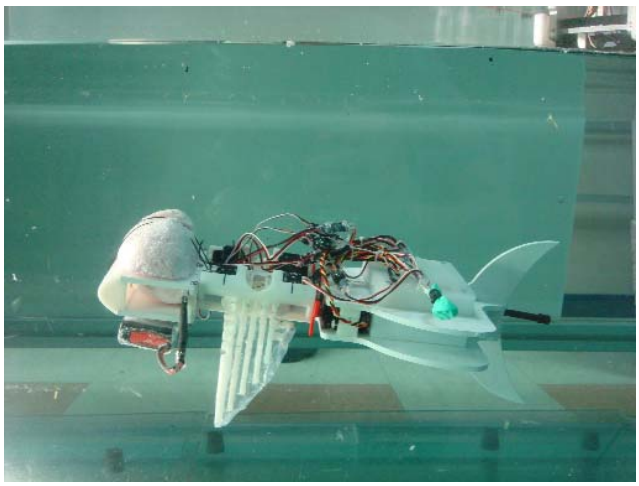

Fig. 7. Vehicle image during straight line maneuver in test tank.

Fin thrust production in CFD was compared with hull drag calculations across a range of vehicle forward speeds to further validate our control simulation model. CFD results in Figure 8 indicate that fin thrust for two fins is equal to vehicle drag at 0.68 knots (0.35 m/s), matching what is seen in simulation.

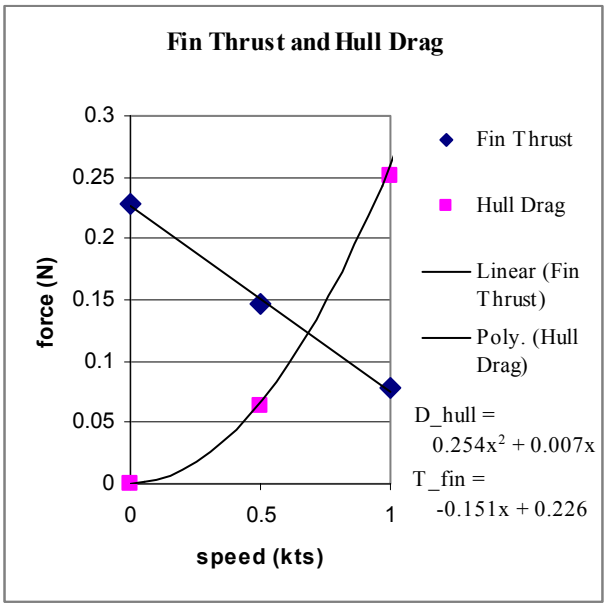

Fig. 8. CFD computed hull drag and fin thrust across a range of vehicle speeds.

The hull drag curve is quadratic as expected. The linear fit to the flapping fin thrust at low speeds is due to the fact that the fin tip speed (~0.5 m/s) is on the same order as the incoming flow speed (ranging from zero to ~0.5 m/s).

4.2. Yaw Maneuver

A yaw maneuver was simulated by commanding the vehicle to turn from a zero degree starting heading to a 180° heading. This turn was completed starting from hover, and simulation shows (Figure 9) the vehicle completed a 180° yaw maneuver in ~10 seconds with an average turn radius of 0.3 meters. Because of the pectoral fins ability to vector their forces in any desired direction, the vehicle completes this heading change through a maneuver about the yaw axis only. No coordinated changes in roll or pitch are needed to achieve a banked turn, and again the EKF holds roll and pitch at their zero degree commanded angles.

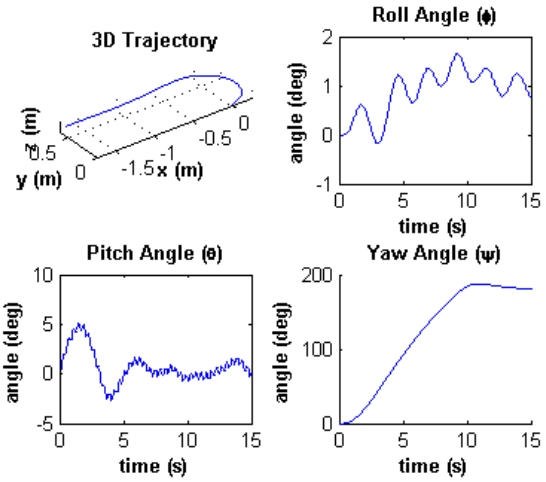

Fig. 9. Simulated 180° heading change in ~10s at 0.3m turn radius.

This simulated turn was duplicated in experimental testing of the vehicle as shown in Figure 10. The turn radius of the vehicle starting from hover was measured at ~0.3 meters with a 90° turn completed in ~6 seconds (~5 seconds in simulation). This slower turn can be attributed to extra vehicle drag associated with the geometry changes which were discussed in Section 4.1.

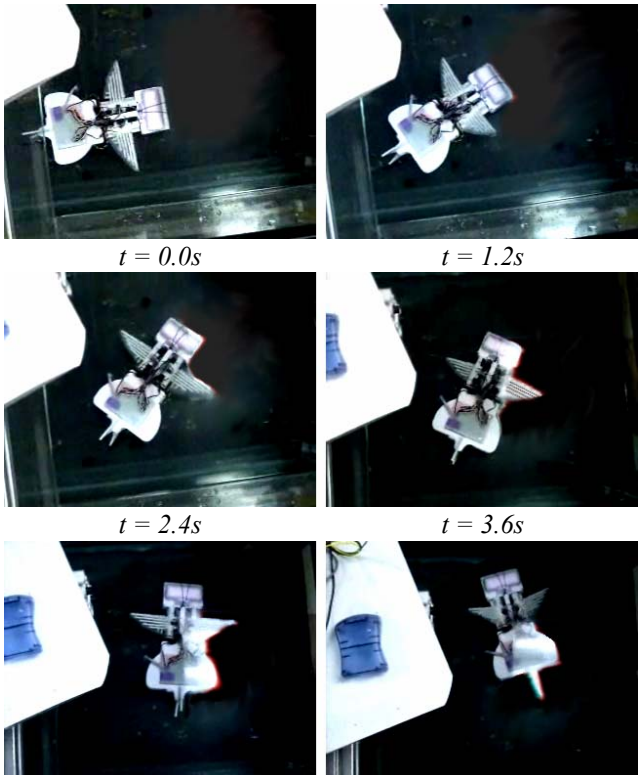

Fig. 10. Vehicle images during yaw maneuver in test tank.

4.3. Climb Maneuver

A climb is induced in simulation to test the pitching response of the vehicle. Results in Figure 11a indicate the vehicle capable of making a 20° pitch change in 3 seconds. This pitch angle is near the maximum inducible pitch for this particular vehicle configuration as indicated by the lift membership curve in Figure 11b. In order to maintain the 20° pitch angle, the fins must be producing close to maximum lift. More details on these membership functions are given by Geder et al (2008).

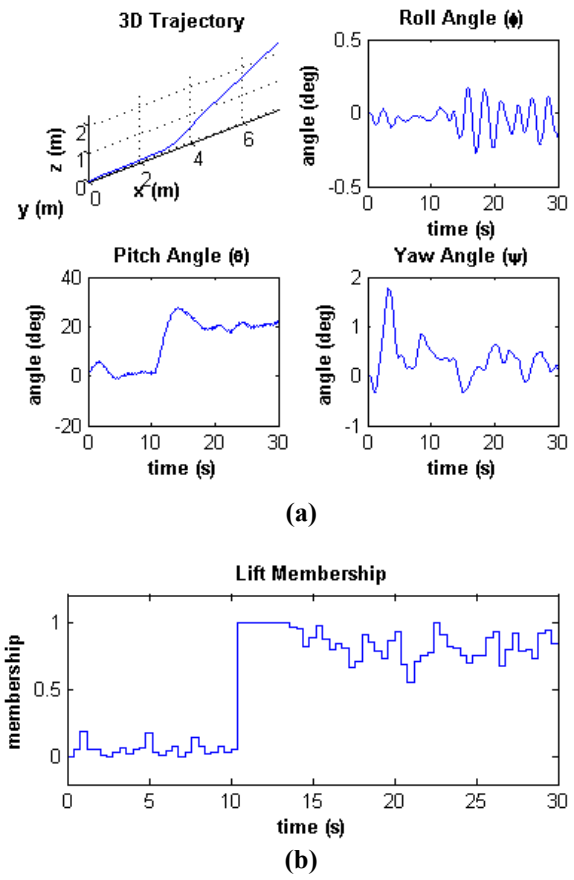

Fig. 11. Simulated 20° climb showing (a) trajectory and attitude control, and (b) lift membership indicating near max lift capability of two-fin vehicle.

These results have yet to be compared with experimental results. More extensive testing of the two-fin vehicle is currently being conducted to display fin capabilities in climbing maneuvers and further validate the vehicle system model used in simulation.

4.4. Controller Robustness

In addition to testing specific maneuvers, the robustness of the vehicle controller with respect to overcoming differences in the actuators has been tested in simulation. To ensure that minor kinematics differences, flaws in fin construction, and mechanical failures do not lead to unstable or uncontrollable behavior, we tested the vehicle response to variations in fin force output (Figure 12).

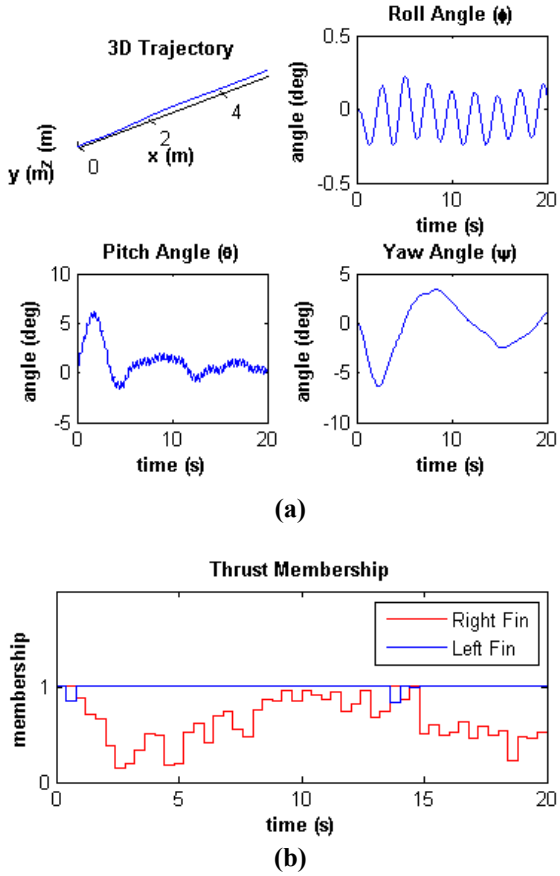

Fig. 12. Simulated straight line test with 50% variation in maximum thrust capability between left and right fins showing (a) trajectory and attitude stability, and (b) thrust membership indicating right left fin working harder to maintain heading.

The straight line test results in Figure 12a show the vehicle response to a forward speed command. In this case the left fin has been compromised in some way, and the maximum output thrust it can generate is two-thirds of the force capability of a properly working right fin. Although the right fin produces 50% more thrust than the left, the controller accounts for this from sensor readings and keeps the heading

on course at zero degrees by reducing the thrust membership of the right fin (Figure 12b).

5. Four-fin Vehicle Design Considerations

Thus far in experimental testing of the two-fin vehicle, results have validated the fidelity of our simulated model of the vehicle. This validation lends confidence to simulation results for other flapping fin vehicle designs, and thus we can use these results to analyze the quality of new vehicle designs for better maneuverability and payload capability.

Based on the results of the two-fin vehicle studies along with preliminary four-fin simulation results, a design for a mission capable four-fin vehicle has been completed. Figure 13 shows a response to a hover command and illustrates the ability of the four-fin to hold a position, something the two-fin vehicle was unable to accomplish stably.

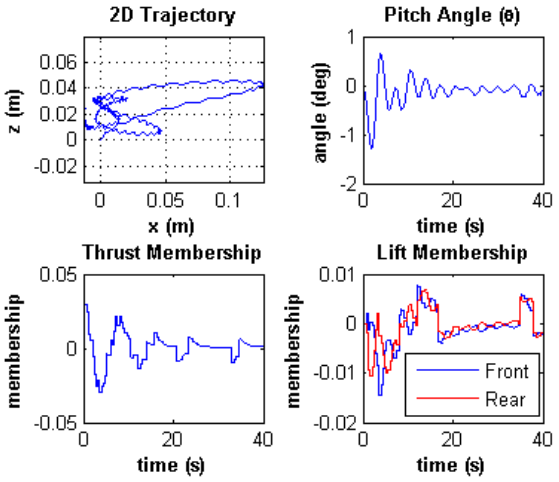

Fig. 13. Four-fin vehicle response to hover command in simulation.

6. Conclusion

An updated vehicle model was presented to include an integrated sensor model. An extended Kalman filter was designed to eliminate attitude drift caused by gyro measurement biases. The successful implementation of this filtering scheme produced desirable results in vehicle maneuvering. Initial experiments were conducted with the two-fin vehicle and results matched those from simulation. This validation of our vehicle model lends confidence to the modeling and simulation of a four-fin vehicle design.

7. Future Work

More extensive testing of the two-fin vehicle is underway. Further results will give us more insight into the capabilities of the flapping fins, and enable us to make improvements to the four-fin vehicle as we continue the design process.

In conjunction with finishing the testing of our two fin vehicle, control algorithms will be adapted to the four-fin vehicle based on our previous studies. Testing of the four-fin vehicle will allow us to not only test maneuvering capabilities with more fins for thrust and control, but also to test onboard cameras and other sensors that are relevant to specific missions.

References

Ando Y, Kato N, Suzuki H, Ariyoshi T, Suzumori K, Kanda T, Endo S, "Elastic Pectoral Fin Actuators for Biomimetic Underwater Vehicles", *Proceedings of the 16th International Offshore and Polar Engineering* Conference, pp. 260-267, 2006.

Eldredge AM, "Improved State Estimation for Miniature Air Vehicles". Masters Thesis, Department of Mechanical Engineering, Brigham Young University, Provo, UT, 2006.

Geder JD, Palmisano J, Ramamurti R, Sandberg WC, Ratna B, "A New Hybrid Approach to Dynamic Modeling and Control Design for a Pectoral Fin Propelled Unmanned Underwater Vehicle", *Proceedings of the International Symposium on Unmanned Untethered Submersible Technology*, Durham, NH, 2007.

Geder JD, Palmisano J, Ramamurti R, Sandberg WC, Ratna B, "Fuzzy Logic PID Based Control and Performance for a Pectoral Fin Propelled Unmanned Underwater Vehicle", *Proceedings of International Conference on Control, Automation and Systems*, Seoul, KR, 2008.

Hobson B, Murray M, Pell CA, "PilotFish: Maximizing Agility in an Unmanned-Underwater Vehicle", *Proceedings of the International Symposium on Unmanned Untethered Submersible Technology*, Durham, NH, 1999.

Kato N, "Hydrodynamic Characteristicsof a Mechanical Pectoral Fin", *Journal of Fluids Engineering, Transactions of the ASME*, vol. 121, pp. 605-613, 1999.

Kato N, “Control Performance of a Fish Robot with Mechanical Pectoral Fins in the Horizontal Plane”, *Journal of Oceanic Engineering, Transactions of the IEEE*, vol. 25, no. 1, 2000.

Lauder GV, Jayne BC, “Pectoral Fin Locomotion in Fishes: Testing Drag-based Models Using Three-dimensional Kinematics”, *American Zoologist*, vol. 36, pp. 567-581, 1996.

Lefferts EJ, Markley FL, Shuster MD, “Kalman Filtering for Spacecraft Attitude Estimation”, *Journal of Guidance, Control, and Dynamics*, vol. 5, no. 5, pp. 417-429, 1982.

Palmisano J, Ramamurti R, Lu K, Cohen J, Sandberg W, Ratna B, “Design of a Biomimetic Controlled-Curvature Robotic Pectoral Fin”, *Proceeding of the IEEE International Conference on Robotics and Automation*, Rome, IT, 2007.

Palmisano J, Geder J, Ramamurti R, Sandberg WC, Ratna B, “Real-time Robotic Pectoral Fin CPG Using Weighted Gait Combinations”, submitted to *IEEE Transactions on Robotics*, in review, 2009.

Ramamurti R, Sandberg WC, “Computational Fluid Dynamics Study for Optimization of a Fin Design”, *AIAA-2006-3658*, San Francisco, CA, 2006.

Ramamurti R, Geder J, Palmisano J, Ratna B, Sandberg WC, “Computations of Flapping Flow Propulsion for UUV Design”, *AIAA-2009-0724*, Washington, DC, 2009.

Tangorra JL, Lauder GV, Madden PG, Mittal R, Bozkurttas M, “A Biorobotic Flapping Fin for Propulsion and Maneuvering”, *Proceedings of the IEEE International Conference on Robotics and Automation*, Rome, IT, 2008.

Uhlmann JK, “Algorithms for multiple-target tracking”, *American Scientist*, vol. 80, pp. 128-141, 1992.

Walker JA, Westneat MW, “Labriform Propulsion in Fishes: Kinematics of Flapping Aquatic Flight in the Bird Wrasse, *Gomphosus Varius* (Labridae)”, *Journal of Experimental Biology*, vol. 200, pp. 1549-1569, 1997.